ORIGINAL PAPER

Synthesis, characterization, and electrochemical application of phosphorus-doped multi-walled carbon nanotubes

**Nikos G. Tsierkezos · Uwe Ritter · Yudi Nugraha Thaha ·
Clive Downing · Paweł Szroeder**

Abstract Phosphorus-doped multi-walled carbon nanotubes (P-MWCNTs) were grown onto oxidized silicon substrate with decomposition of cyclohexane (CyH) and triphenylphosphine (TPP) in the presence of ferrocene (FeCp$_2$) by means of chemical vapor deposition technique. For the fabrication, the mass percent of TPP in CyH/TPP/FeCp$_2$ ternary mixture was varied from 0.5 % to 2.0 % wt., while the mass percent of FeCp$_2$ was fixed to either 2.0 % or 5.0 % wt. The P-MWCNTs were characterized using scanning and transmission electron microscopy in combination with energy-dispersive X-ray spectroscopy as well as using Raman spectroscopy. The electrochemical response of P-MWCNTs towards ferrocyanide/ferricyanide [Fe(CN)$_6$]$^{3-/4-}$ was studied by means of cyclic voltammetry and electrochemical impedance spectroscopy. Application of P-MWCNTs for electrochemical analysis of ascorbic acid (AA), dopamine (DA), and uric acid (UA) was successfully carried out, and limits of detection of 1.12 μM, 0.19 μM, and 0.80 μM were estimated, respectively. The findings demonstrate that P-MWCNTs are a quite promising material for applications in electrochemical sensing.

Introduction

Multi-walled carbon nanotubes (MWCNTs) are considered very promising and attractive nanomaterials for various applications in electroanalysis due to their marvelous electrical, chemical, and mechanical properties [1]. Thus, MWCNTs were extensively used for the construction of composite electrodes and precise electrochemical devices since they enhance the kinetic of redox processes and improve the sensitivity of sensing systems due to their large surface area and their high electrical conductivity [2, 3]. According to literature reports, novel composite electrodes based on MWCNTs were already extensively applied with great electrochemical performance for the analysis of various redox systems of great interest [4–6].

The warp of carbon nanotubes modifies the chemically inert graphite surface and permits the incorporation of elements in their structure. Accordingly, the inclusion of non-carbon atoms into the hexagonal network of carbon nanotubes modifies the electronic and chemical properties due to variations in electronic structure [7]. It is remarkable that the doped sites within carbon nanotubes modify significantly their chemical reactivity, thereby broadening the spectrum of their possible applications, especially in the field of electrochemical sensing. Nitrogen that is known to have low doping levels in bulk graphite can be easily incorporated into the structure of carbon nanotubes by substitution. Nitrogen acts as an electron donor in carbon nanotubes, since it has five valence electrons,

N. G. Tsierkezos (✉) · U. Ritter · Y. N. Thaha
Department of Chemistry, Institute of Chemistry and Biotechnology, Ilmenau University of Technology, Weimarer Straße 25, 98693 Ilmenau, Germany
e-mail: nikos.tsierkezos@tu-ilmenau.de

P. Szroeder
Institute of Physics, Faculty of Physics, Astronomy and Informatics, Nicolaus Copernicus University, Grudziadzka 5, 87-100 Toruń, Poland

C. Downing
Advanced Microscopy Laboratory, CRANN, Trinity College Dublin, Dublin 2, Ireland

causing a shift in the Fermi level to the conduction bands, and therefore making all nitrogen-doped tubes metallic, regardless of their geometry. As was already reported in literature, nitrogen can be incorporated within carbon nanotubes in pyridine-like fashion [8]. Phosphorus can be also effectively incorporated into carbon nanotubes either as single substitution dopant [9] or as co-dopant along with nitrogen [10]. Theoretical investigations showed that both phosphorus and phosphorus-nitrogen defects are characterized by the presence of highly localized state close to the Fermi level, a promising evidence for notorious chemical reactivity and great electrochemical sensing capability [11].

The aim of the present work is the production of phosphorus-doped carbon nanotubes, their electron microscopic, Raman spectroscopic, and electrochemical characterization and their application in electrochemical sensing. Phosphorus-doped multi-walled carbon nanotubes (P-MWCNTs) were fabricated by means of chemical vapor deposition (CVD) technique with decomposition of cyclohexane (CyH) and triphenylphosphine (TPP) onto oxidized silicon substrate in the presence of ferrocene ($FeCp_2$). For the fabrication of P-MWCNTs, four different compositions of TPP/CyH/$FeCp_2$ ternary mixtures were used. The P-MWCNTs films were characterized by means of scanning electron microscopy (SEM) and transmission electron microscopy (TEM) in combination with energy-dispersive X-ray spectroscopy (EDX) as well as with Raman spectroscopy. Furthermore, the electrochemical response of P-MWCNTs towards the standard redox system ferrocyanide/ferricyanide $[Fe(CN)_6]^{3-/4-}$ was studied in aqueous potassium chloride solution by means of cyclic voltammetry (CV) and electrochemical impedance spectroscopy (EIS) techniques. Application of P-MWCNTs for electrochemical analysis of ascorbic acid (AA), dopamine (DA), and uric acid (UA) in phosphate buffer solution (pH 7.0) was also carried out.

Experimental

Chemicals and solutions

Triphenylphosphine (>99 %), cyclohexane (>99 %), ferrocene (>98 %), potassium hexacyanoferrate(III), (>99.0 %), potassium hexacyanoferrate(II) trihydrate, (>98.5 %), dopamine (>99.0 %), and potassium chloride (>99.0 %) were purchased from Sigma-Aldrich, while L(+)-ascorbic acid (99.7 %) and uric acid (≥98 %) were purchased from Merck and Fluka, respectively. All chemicals were used as received without any further purification. For the electrochemistry measurements, a stock solution of $K_3Fe(CN)_6$/$K_4Fe(CN)_6$ binary mixture with concentration of 1.0×10^{-2} M was prepared by dissolving the appropriate amounts of salts in 1.0 M KCl aqueous solution. The stock

solution of $[Fe(CN)_6]^{3-/4-}$ was prepared immediately prior the electrochemical experiments by using high-quality distilled water. The measured solutions of $[Fe(CN)_6]^{3-/4-}$ in concentration range of 0.099-0.990 mM, were prepared directly in electrochemical cell with progressive addition of appropriate volume of stock solution in 1.0 M aqueous KCl solution. The solutions of AA, DA, and UA of the desired concentration were prepared immediately prior to the electrochemical experiments by using phosphate buffer solution (pH 7.0). The electrochemistry experiments were carried out at the room temperature.

Fabrication of P-MWCNTs composite films

The growth of P-MWCNTs onto silicon/silicon oxide substrate was carried out successfully by means of CVD technique with decomposition of CyH (carbon source material) and TPP (phosphorus source material) in the presence of $FeCp_2$ (catalyst). The mass percent of TPP and $FeCp_2$ in TPP/CyH/$FeCp_2$ ternary mixture was varied in order to find the optimum experimental conditions for the production of high quality phosphor-doped carbon nanotubes. Specifically, the mass percent of TPP in the TPP/CyH/$FeCp_2$ ternary mixture was varied in the range of 0.5-2.0 % wt., while the mass percent of $FeCp_2$ was fixed to either 2.0 % or 5.0 % wt. (Table S1; Supporting Information). For the growth process, the TPP/CyH/$FeCp_2$ ternary mixture was introduced to the furnace at the temperature of 900 °C through a syringe with a flow rate of 0.17 mL min^{-1} (the growth processing time was fixed at about 18 min). In case of P-MWCNTs film fabricated with the smallest mass percent of TPP (0.5 % wt. TPP), three different pyrolysis experiments were carried out in order to produce electrochemically active samples by spraying 3, 4 and 5 mL of TPP/CyH/$FeCp_2$ ternary mixture (growing times of about 18, 24, and 29 min, respectively). It is quite interesting that the P-MWCNTs films fabricated by spraying 3 and 4 mL of ternary mixture exhibited rather disturbed CVs and thus they could not be used for sensing purposes (Fig. S1; Supporting Information). The scheme of CVD apparatus and experimental details concerning the pyrolysis technique were already reported in previous published articles [12, 13]. The P-MWCNTs-based working electrodes for electrochemistry measurements were prepared as follows: the fabricated P-MWCNTs films were initially connected to platinum wire by using silver conducting coating, and once the silver coating was dried, the silver conducting part of P-MWCNTs composite films was fully covered with varnish protective coating [14].

Instrumentation

The electrochemical measurements were carried out on electrochemical working station Zahner (IM6/6EX,

Germany) and the obtained data were analyzed by means of Thales software (version 4.15). A three electrode system consisting of P-MWCNTs-based working electrode, platinum plate counter electrode, silver/silver chloride (saturated KCl) reference electrode was used for electrochemistry measurements. The electrochemical impedance spectra were recorded in the frequency range from 0.1 Hz to 100 kHz at the half-wave potential of studied redox system $[Fe(CN)_6]^{3-/4-}$ ($E_{1/2}$=+0.275 V vs. Ag/AgCl). All electrochemistry measurements were carried out at the room temperature. All solutions were deoxygenated by purging with high-purity nitrogen for ten minutes prior to measurement. More details regarding the electrochemistry measurements were already reported in previous published articles [15–17]. The morphology and elemental composition of various produced P-MWCNTs films were examined by transmission electron microscope (FEI Titan operating at 300kv, images acquired using TEM and elemental analysis aquired using STEM), and scanning electron microscope (Zeiss Ultra with an oxford instruments EDX detector) equipped with an energy dispersive X-ray spectrometer [18]. Raman spectra of various P-MWCNTs films were recorded using inVia microprobe spectrometer (Renishow, Gloucestershire, UK) coupled to Leica confocal microscope. Laser excitation light of the length of 488 nm and power of about 20 mW was used. The diameter of the laser spot was about 1 μm. The main Raman modes characteristic to sp^2-carbon materials were fitted using Lorentzian curves.

Results and discussion

Scanning electron microscopic and transmission electron microscopic analysis

Representative SEM and TEM images of various fabricated P-MWCNTs composite films are shown in Figs. 1 and 2, respectively. Furthermore, representative EDX spectra recorded for the various P-MWCNTs composite films are shown in Figs. S2-S5 (Supporting Information). The P-MWCNTs-1 and P-MWCNTs-4 films contain carbon nanotubes that are highly phosphorus-iron doped and are quite long. Especially in P-MWCNTs-1 film sole carbon nanotubes can be clearly recognized in TEM micrographs having length in the range of 2.0-4.0 μm and inner and outer diameter of about 20 and 40 nm, respectively. The structure of carbon nanotubes in P-MWCNTs-1 and P-MWCNTs-4 samples consist of "closed" room-spaces divided with numerous carbon nanowalls that are either empty of completely filled with iron-phosphorus nanoparticles. The structure of these nanotubes is similar in some

way to that of the nitrogen-doped nanotubes, which they possess the so-called bamboo-shaped structure. It must be mentioned, however, that the structure of the carbon nanotubes breaks down at the end of the longer tubes. According to published work of Jourdain et al. [19], the bamboo morphology appears to be correlated with the diameter of the catalytic nanoparticles. The TEM/EDX analysis of P-MWCNTs-1 and P-MWCNTs-4 confirms that the nanotubes are filled with iron-phosphorus nanoparticles. In P-MWCNTs-2 and P-MWCNTs-3 composite films sole carbon nanotubes cannot be clearly recognized and the most of the species that can be seen are great adducts (clusters) of carbon nanotubes that cannot be parted to single nanotubes upon sonication. The P-MWCNTs-2 and P-MWCNTs-3 films consist mostly of aggregates of carbon nanotubes that are also highly phosphorus-iron doped. In the P-MWCNTs-2 and P-MWCNTs-3 films phosphorus-iron nanoparticles, which are wrapped with numerous layers of graphitic carbon, can be also seen in TEM images. These wrapped with nanotubes phosphorus-iron nanoparticles, which look like "onions", probably resulted from demolished structure of carbon nanotubes. It is very interesting to mention that according to EDX analysis the overall phosphorus incorporated into carbon nanotubes was between 1-2 % wt. for all studied P-MWCNTs composite films, independently of mass percent of TPP used for the production of P-MWCNTs. Larrude et al. [20] performed X-ray photoelectron spectroscopy (XPS) studies of P-MWCNTs produced by means of spray pyrolysis using TPP/FeCp$_2$ in toluene. The XPS findings demonstrated the chemical environment of phosphorus atoms and confirmed the presence of substitutional phosphorus in the structure of carbon nanotubes. Furthermore, Cruz-Silva et al. [10] reported that the most of metallic nanoparticles in P-MWCNTs produced with pyrolysis of TPP/FeCp$_2$ are primarily composed of iron and phosphorus (iron phosphide nanoparticles) and only small amount of metallic particles covered by amorphous carbon do not contain phosphorus (these are either iron or iron carbide nanoparticles). Cruz-Silva et al. [10] using ab initio calculations have shown that phosphorus can exist as dopant (along with nitrogen) within the carbon nanotubes walls.

Raman spectroscopic analysis

Raman spectra recorded for P-MWCNTs are shown in Fig. 3. Three main Raman features, G, G', and D, characteristic to the sp^2-bonded carbons, were fitted with a Lorentzian peak shape. The results of the fitting procedure are compared in Table 1. Strong correlation between the position of the Raman peaks and concentration of TPP in the nanotube growth precursor is observed. The finding demonstrate that the peaks red-shifted with the increase of concentration of TPP. The red-shift of the

Fig. 1 SEM micrographs of P-MWCNTs-1 (**a,b**), P-MWCNTs-2 (**c,d**), P-MWCNTs-3 (**e,f**), and P-MWCNTs-4 (**g,h**) composite films taken with accelerating voltage of 3 kV and magnification factors in the range of 1.0×10^4–9.0×10^4
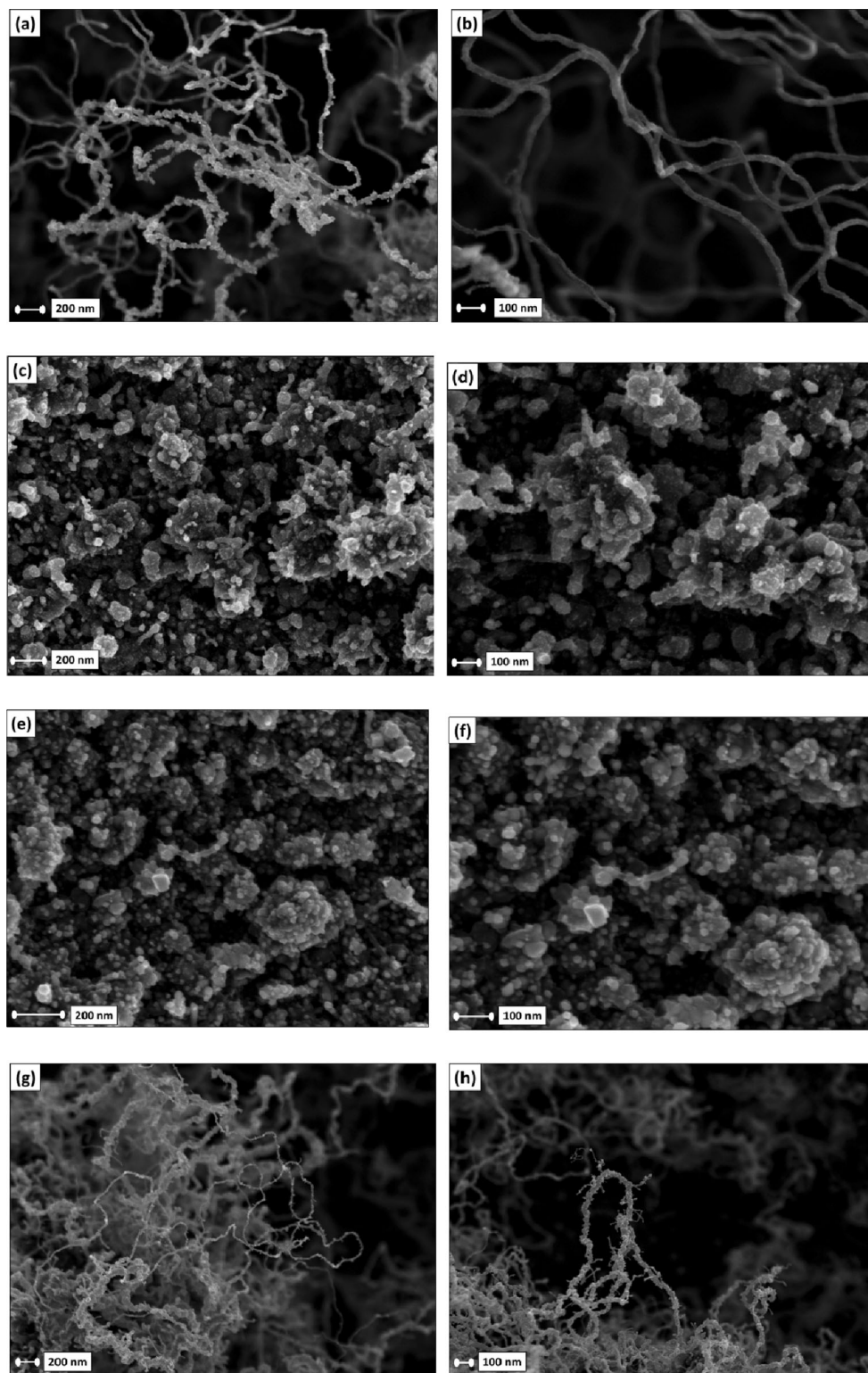
Raman bands is probably induced by softening of the force constants and donor doping [21]. However at the concentration of 2 % downshift disappeared. In the recorded spectra, relatively strong disorder induced D-mode appears. It has been shown that, the relative intensity of D and G lines, as well as G' and G lines is a measure of disorder and number of graphene layers in low dimensional carbons [22–25]. Intensity ratio of D and G bands, I_D/I_G, attained the lowest value in carbon nanotubes grown at the concentration of TPP of 1 %. Using procedure described in our previous published

Fig. 2 TEM micrographs of P-MWCNTs-1 (**a-c**), P-MWCNTs-2 (**d-f**), P-MWCNTs-3 (**g-i**), and P-MWCNTs-4 (**j-l**) composite films
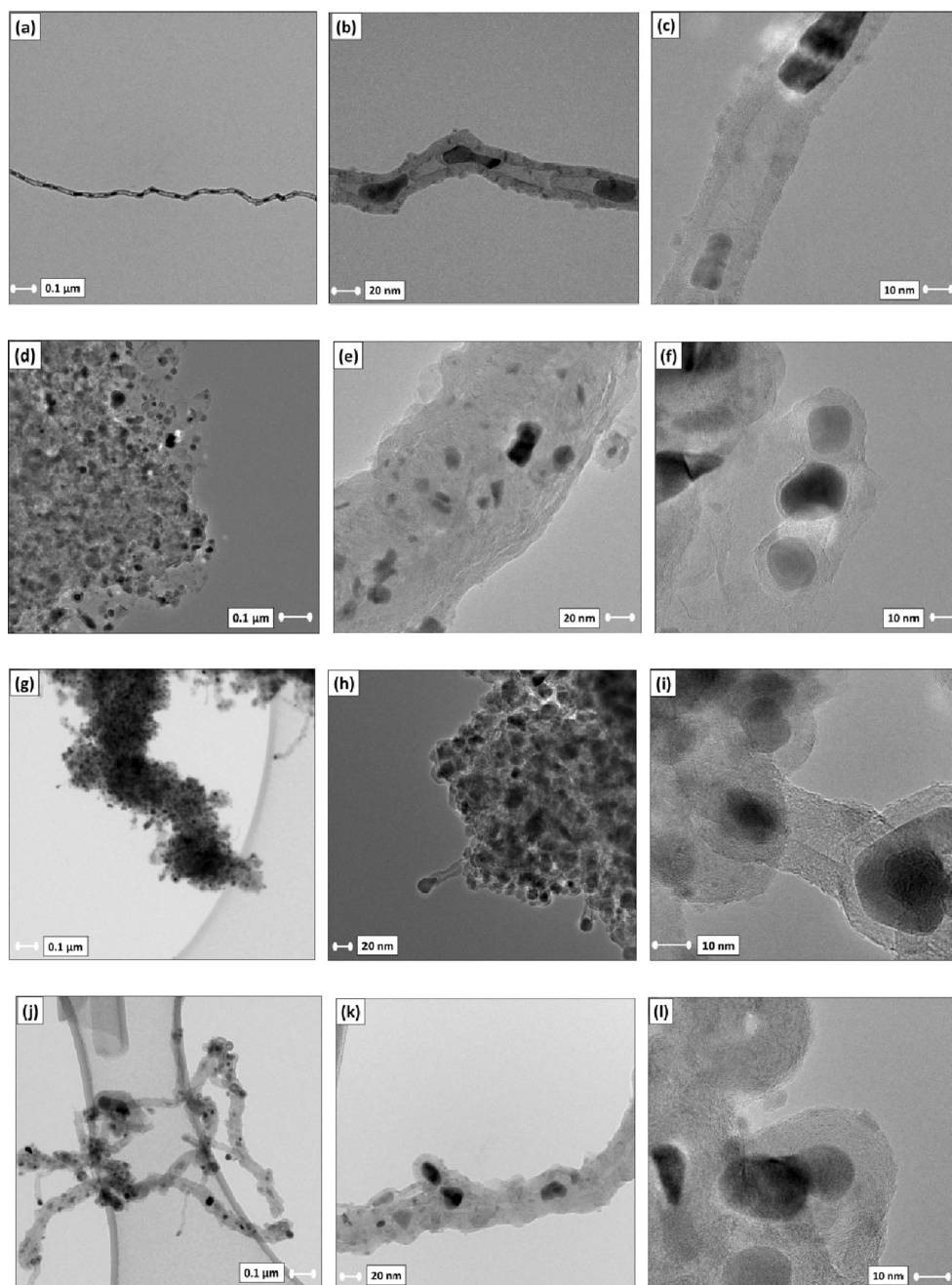

manuscript [26], the average distance between defects can be estimated to 14 ± 1 nm and 12 ± 1 nm for carbon nanotubes grown with 0.5 % and 1 % of TPP, respectively. It is interesting to mention that the increased concentration of FeCp$_2$ in growth precursor of P-MWCNTs-1 relative to P-MWCNTs-2 does not influence the shape of main Raman features, demonstrating, therefore, that the degree of defects in P-MWCNTs-1 and P-MWCNTs-2 films is comparable. On the other hand, higher content of adducts in P-MWCNTs-2 film is clearly seen in SEM and TEM images. This concerns also the sample P-MWCNTs-3, where tubular sp^2 carbon structures are almost not visible. It leads us to the conclusion, that excess

of TPP relative to FeCp$_2$ can supress the MWCNTs growth and does not cause the higher concentration of phosphorus in sp^2-bonded carbon tubules. This observation can be probably related to the poisoning of metallic catalyst particles, and consequently, to the declining of their catalytic activity with increasing of TPP concentration [19, 27].

Electrochemical characterization and application in sensing

The potential application of fabricated novel P-MWCNTs films as electrode materials was tested with standard techniques such as CV and EIS. CVs recorded for [Fe(CN)$_6$]$^{3-/4-}$
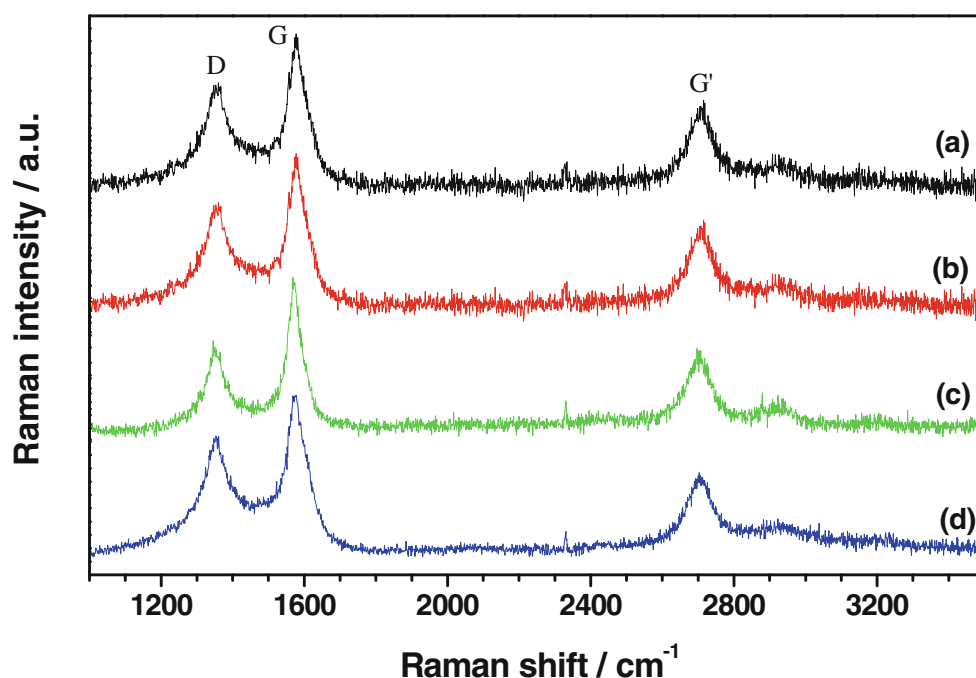
(1.0 M KCl) on various P-MWCNTs composite films at the scan rate of 0.02 V s^{-1} showing the effect of variation of concentration of redox system in the range of 0.099–0.990 mM are shown in Fig. 4. The change of oxidation current of redox system $[Fe(CN)_6]^{3-/4-}$ with the variation of its concentration on various P-MWCNTs films is presented graphically in Fig. S6 (Supporting Information). The esti-mated electrochemical and kinetic parameters of $[Fe(CN)_6]^{3-/4-}$ on various P-MWCNTs composite films are presented in Table 2. The CVs recorded on P-MWCNTs films are quite symmetric and consist of two well-defined reversible anodic and cathodic waves lying at about $E_p^{ox} \approx$ 0.32 V (vs. Ag/AgCl) and $E_p^{red} \approx 0.22$ V (vs. Ag/AgCl), respectively, which correspond to the one-electron transfer process involving the standard redox system $[Fe(CN)_6]^{3-/4-}$. The half-wave potential of $[Fe(CN)_6]^{3-/4-}$ on P-MWCNTs films lies at about $E_{1/2} \approx 0.275$ V (vs. Ag/AgCl) and is independent on electrode's material, something that is ex-pectable for reversible redox systems. The CVs recorded on P-MWCNTs are quite symmetric, and thus, the peak current ratio of oxidation and reduction peaks is equal to unity and is independent of scan rate demonstrating that there are no

parallel chemical reactions coupled to the electrochemical process. In addition, the oxidative and reductive peak cur-rents are essentially constant after recording several cycles (no loss of electroactivity was observed for recording con-tinuously 50 cycles). This finding demonstrates that there are no chemical reactions coupled to electron transfer and that the redox system $[Fe(CN)_6]^{3-/4-}$ is stable in the time frame of experiment confirming that the charge-transfer process occurring on novel P-MWCNTs films is reversible. The effect of variation of scan rate on oxidation peak current of $[Fe(CN)_6]^{3-/4-}$ shows a linear variation of peak current with the square root of scan rate indicating that the electrochemical process occurring onto novel P-MWCNTs films is diffusion controlled. This finding is another evi-dence of the reversibility of investigated $[Fe(CN)_6]^{3-/4-}$ redox couple onto novel P-MWCNTs composite films. As an example, representative CVs recorded for $[Fe(CN)_6]^{3-/4-}$ at various scan rates (in the range of 0.02–0.12 V s^{-1}) on P-MWCNTs-1 film along with the variation of oxidation current of $[Fe(CN)_6]^{3-/4-}$ with the square root of scan rate are shown in Fig. S7 (Supporting Information). The values of anodic and cathodic peak potential separation ($\Delta E_p =$

Table 1 Positions of D, G, and G' Raman bands, intensity ratios of D and G bands (I_D/I_G), and integral intensity ratios of G' and G bands ($A_{G'}/A_G$) for P-MWCNTs-1, P-MWCNTs-2, P-MWCNTs-3, and P-MWCNTs-4 composite films

Material	D/cm^{-1}	G/cm^{-1}	G'/cm^{-1}	I_D/I_G	$A_{G'}/A_G$
P-MWCNTs-1	1355.0±0.8	1579.3±0.4	2707.9±0.7	0.66±0.03	0.58±0.03
P-MWCNTs-2	1355.0±0.8	1579.3±0.4	2707.9±0.7	0.66±0.03	0.58±0.03
P-MWCNTs-3	1352.6±0.6	1572.1±0.3	2701.5±0.6	0.53±0.2	0.65±0.02
P-MWCNTs-4	1355.0±0.6	1576.7±0.3	2704.5±0.6	0.68±0.2	0.39±0.02

Fig. 4 CVs recorded for various concentrations of $[Fe(CN)_6]^{3-/4-}$ (1.0 M KCl) on P-MWCNTs-1 (**a**), P-MWCNTs-2 (**b**), P-MWCNTs-3 (**c**), and P-MWCNTs-4 (**d**) composite films at the scan rate of $0.02\ V\cdot s^{-1}$. The CVs (from inner to outer) correspond to the following concentrations: $c_1=0.099$ mM; $c_2=0.196$ mM; $c_3=0.291$ mM; $c_4=0.415$ mM; $c_5=0.506$ mM; $c_6=0.595$ mM; $c_7=0.712$ mM; $c_8=0.797$ mM; $c_9=0.909$ mM; $c_{10}=0.990$ mM
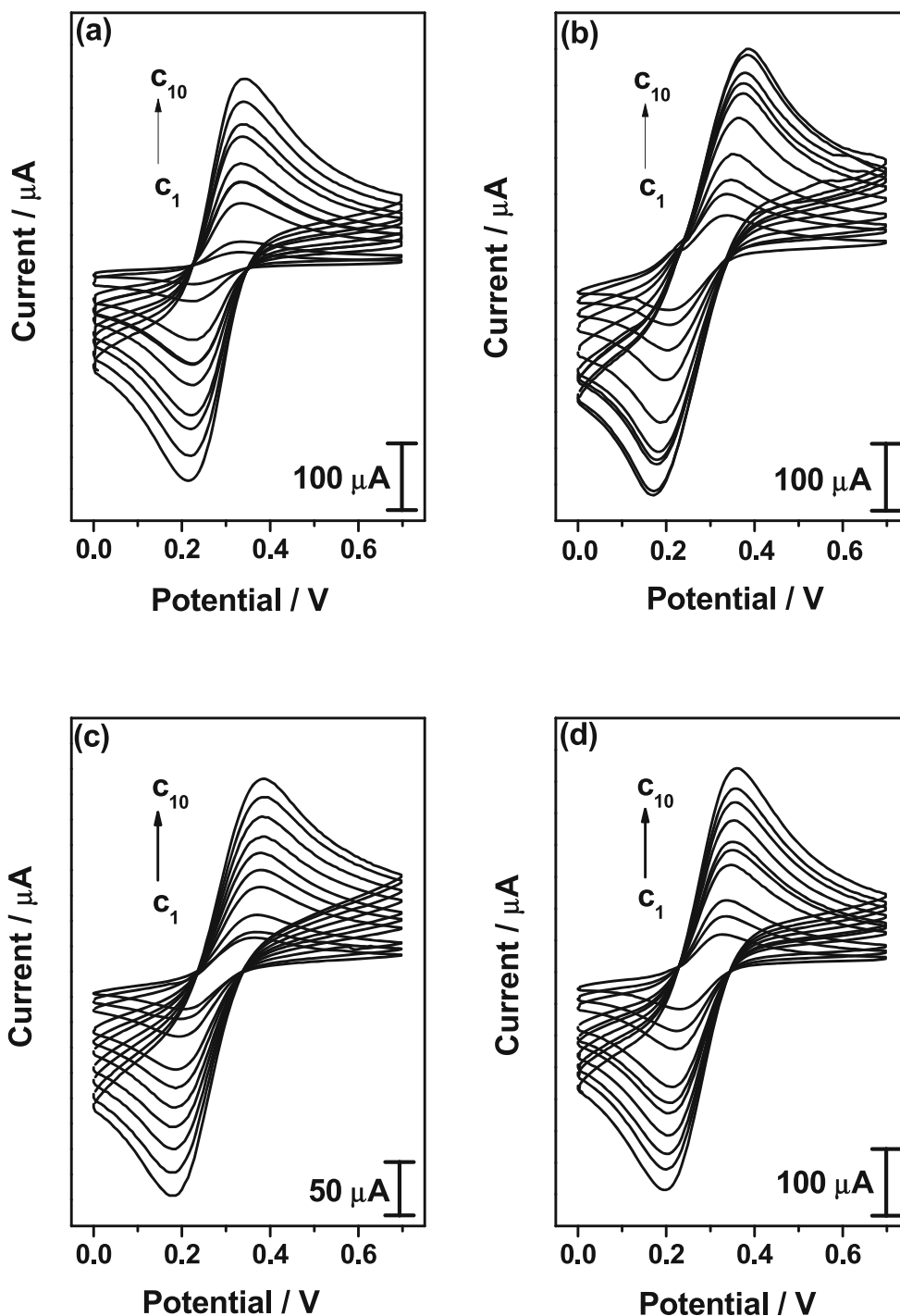
$E_p^{ox}-E_p^{red}$) obtained for $[Fe(CN)_6]^{3-/4-}$ on various P-MWCNTs films appear to be strongly dependent on working electrode's material as well as on concentration of redox system (the ΔE_p values tend to increase slightly with the increase of concentration). Furthermore, the ΔE_p values are greater compared to the ideal value of $\Delta E_p=0.059$ V [28], which is indicative of reversible one-electron transfer redox process. Since the peak separation due to electron transfer kinetics must be constant with the concentration of redox

system (at a given scan rate), the increase in peak potential separation with the rise in concentration of redox system (and thus with the increase of oxidation and reduction peak currents) can be attributed to uncompensated resistance effect. Solak et al. [29] reported that the "observed" ΔE_p value for redox system is the sum of the "corrected" ΔE_p value and the term $2i_p R_u$, where i_p is the oxidation or reduction peak current and R_u represents the uncompensated resistance. Consequently, the corrected ΔE_p value can

Table 2 Anodic peak potential (E_p^{ox}), cathodic peak potential (E_p^{red}), half-wave potential ($E_{1/2}$), observed (ΔE_p^{obs}) and corrected (ΔE_p^{corr}) anodic and cathodic peak potential separation, anodic and cathodic peak current ratio (i_p^{ox}/i_p^{red}), heterogeneous electron transfer rate constant (k_s), charge transfer resistance (R_{ct}), lower limit of detection (LOD), and sensitivity (S) for P-MWCNTs-1, P-MWCNTs-2, P-MWCNTs-3, and P-MWCNTs-4 composite films towards $[Fe(CN)_6]^{3-/4-}$ (1.0 M KCl)

Parameters	P-MWCNTs-1	P-MWCNTs-2	P-MWCNTs-3	P-MWCNTs-4
E_p^{ox}/V	0.321	0.333	0.357	0.326
E_p^{red}/V	0.231	0.213	0.194	0.228
$E_{1/2}$/V	0.276	0.273	0.276	0.277
ΔE_p^{obs}/V	0.090	0.120	0.163	0.098
ΔE_p^{corr}/V	0.073	0.091	0.119	0.079
i_p^{ox}/i_p^{red}/A	1.01	1.01	1.01	0.99
$k_s/10^{-3}$ cm·s^{-1}	7.36	3.64	1.55	5.72
R_{ct}/Ω	13	142	895	46
LOD/μM	0.60	0.65	0.83	0.63
S/A·M^{-1}·cm^{-2}	0.301	0.278	0.184	0.289

be graphically estimated as the intercept of the plot of observed ΔE_p versus i_p (with slope $2R_u$). As an example, representative plots showing the variation of ΔE_p with the oxidation current of $[Fe(CN)_6]^{3-/4-}$ in the concentration range of 0.099–0.990 mM on two different P-MWCNTs composite films are presented in Fig. S8 (Supporting Information). The corrected ΔE_p values corresponding to "no effect" of concentration of electroactive species are included in Table 2 along with the observed ΔE_p values for comparison reasons. As it can be observed in Table 2, the corrected ΔE_p values of $[Fe(CN)_6]^{3-/4-}$ on P-MWCNTs-1, P-MWCNTs-2, P-MWCNTs-3, and P-MWCNTs-4 films appear to be smaller for about 18 %, 24 %, 27 %, and 19 %, respectively, compared to the corresponding observed ΔE_p values. This finding demonstrates the great incorrectness of kinetic parameters that would result from the interpretation of the observed ΔE_p values. Based on the degree of the peak potential separation between the forward and reverse scans (the corrected ΔE_p values), the heterogeneous electron transfer rate constants (k_s) can be estimated by means of electrochemical absolute rate relation. Namely, in order to determine the heterogeneous electron transfer rate constants of $[Fe(CN)_6]^{3-/4-}$ system on P-MWCNTs films, the procedure suggested by Nicholson [30], which relates k_s with ΔE_p through a working curve of dimensionless kinetic parameter ψ, was applied. For the determination of k_s, the diffusion coefficient of $[Fe(CN)_6]^{3-/4-}$ was taken as $D = 7.2 \times 10^{-6}$ cm^2·s^{-1} [31]. The determined k_s values of $[Fe(CN)_6]^{3-/4-}$ on various fabricated P-MWCNTs films are included in Table 2. The findings demonstrate slight differences of kinetic of redox process involving $[Fe(CN)_6]^{3-/4-}$ on various P-MWCNTs composite films. Specifically, the rate for electron transfer of $[Fe(CN)_6]^{3-/4-}$ on P-MWCNTs films tends to increase with the following order: P-MWCNTs-3 < P-MWCNTs-2 < P-MWCNTs-4 < P-MWCNTs-1. The findings demonstrate that the P-MWCNTs-1 and P-MWCNTs-4 composite films, consisting of long and sole "bamboo-shaped" carbon

nanotubes, approve somehow the electron transfer kinetic of $[Fe(CN)_6]^{3-/4-}$ system. In contrast, on P-MWCNTs-2 and P-MWCNTs-3 films, consisting of clustered nanotubes, the electron-transfer kinetic appears to be slower.

In order to estimate the detection ability and sensitivity of various P-MWCNTs composite films towards $[Fe(CN)_6]^{3-/4-}$, the variation of oxidation peak current with the concentration of redox system was considered. The findings demonstrate that the fabricated novel P-MWCNTs films exhibit linear current response towards $[Fe(CN)_6]^{3-/4-}$ in the investigated concentration range of 0.099–0.990 mM (Fig. S6; Supporting Information). From the linear concentration-current calibration curves, the lower limits of detection as well as the sensitivities of novel P-MWCNTs films towards $[Fe(CN)_6]^{3-/4-}$ were estimated and are included in Table 2. The findings exhibit that the sensitivity and detection ability of novel films tend to enhance with the following order: P-MWCNTs-3 < P-MWCNTs-2 < P-MWCNTs-4 < P-MWCNTs-1. It is very interesting that with the same order, the kinetic of electron transfer reaction increases. This finding exhibits an improvement of sensitivity of P-MWCNTs films consisting of sole non-clustered carbon nanotubes. It would be very interesting to compare the lower limit of detection of P-MWCNTs films towards $[Fe(CN)_6]^{3-/4-}$ with those reported in literature for other novel composite films. This comparison, which is presented in Table S2 (Supporting Information), shows clearly that the P-MWCNTs composite films exhibit greater detection capability towards the redox couple $[Fe(CN)_6]^{3-/4-}$ compared to other novel films reported in literature. These findings exhibit the excellent electro-catalytic performance of P-MWCNTs composite films. Furthermore, it is remarkable that the phosphorus-doping appears to improve the detection ability of carbon nanotubes towards $[Fe(CN)_6]^{3-/4-}$. As it can be seen in Table S2 (Supporting Information), the detection ability of carbon nanotubes which incorporate phosphorus into their structure appears to be about 47–62 % greater compared to that

of pristine un-doped carbon nanotubes. Nevertheless, it must be mentioned that the phosphorus doping of carbon nanotubes cannot compete the nitrogen doping of the tubes that improves even more the detection ability of carbon nanotubes towards $[Fe(CN)_6]^{3-/4-}$ (an improvement of detection limit of about 70 % is observed upon nitrogen doping of nanotubes). These findings confirm the particularly enhanced electrocatalytic properties of carbon nanotubes that incorporate nitrogen atoms into their structure [32, 33]. According to literature reports, the extra valence electrons of dopant material occupy the carbon nanotubes

conduction band and shift the Fermi level towards the conduction band improving the conductivity of carbon nanotubes and enhancing their electrochemical response [34].

The electrochemical behavior of redox system $[Fe(CN)_6]^{3-/4-}$ on novel P-MWCNTs films was further investigated by means of EIS technique. Representative EIS spectra recorded for $[Fe(CN)_6]^{3-/4-}$ on various P-MWCNTs composite films in the frequency range of 0.10 Hz–100 kHz are displayed in Fig. 5. In EIS spectra, which are displayed as Nyquist plots, the complex impedance of

Fig. 5 EIS spectra recorded for 0.099 mM $[Fe(CN)_6]^{3-/4-}$ (1.0 M KCl) on P-MWCNTs-1 (**a**), P-MWCNTs-2 (**b**), P-MWCNTs-3 (**c**), and P-MWCNTs-4 (**d**) composite films. The EIS spectra were recorded at the half-wave potential of the studied redox system $[Fe(CN)_6]^{3-/4-}$ ($E_{1/2}$=+0.280 V vs. Ag/AgCl) in the frequency range of 0.10 Hz-100 kHz
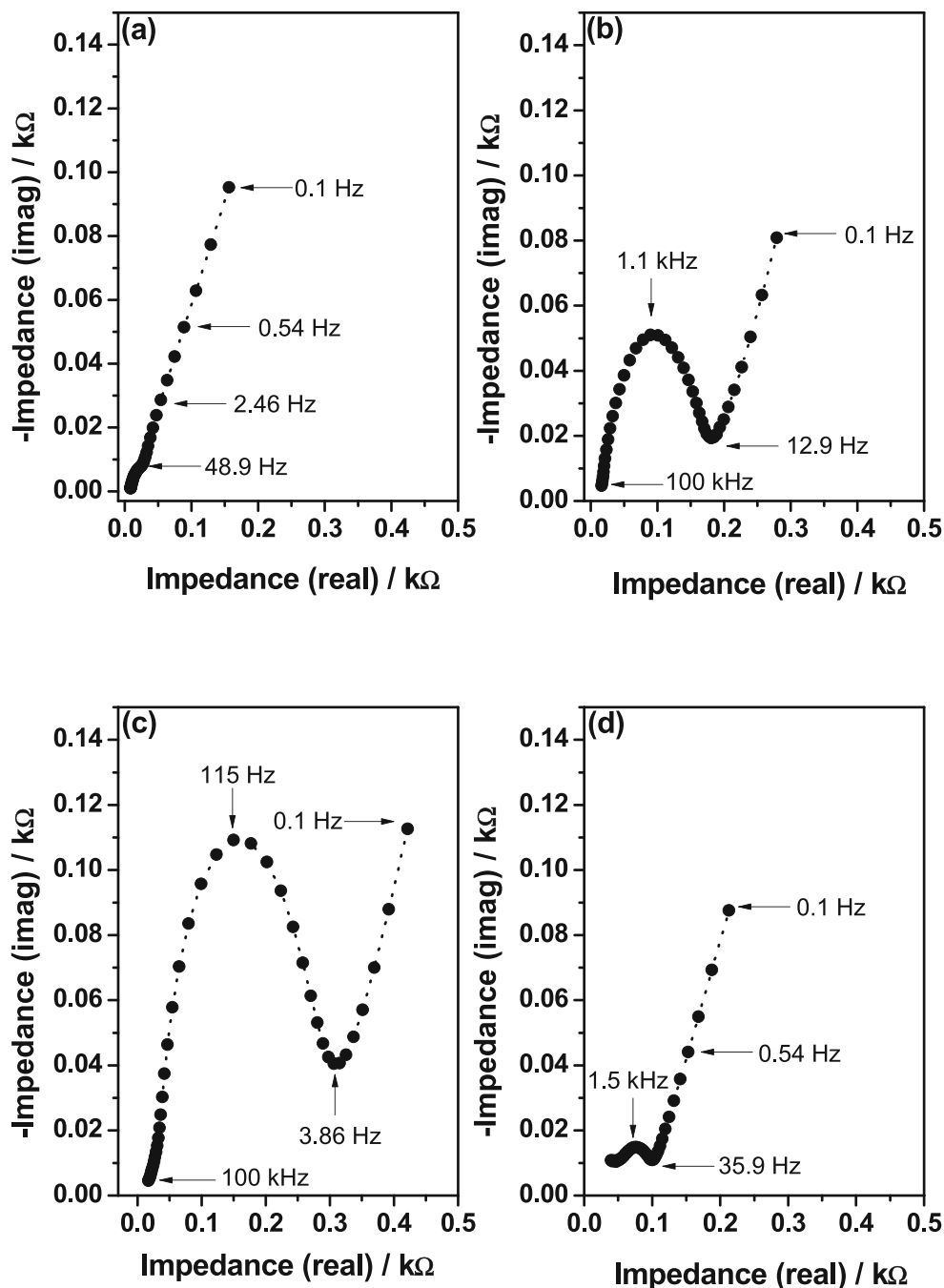
studied system is presented as the sum of the real and the imaginary impedance components (impedance values in x- and y-axis, respectively). The recorded EIS spectra reveal that the impedance is controlled by the interfacial electron transfer at high frequencies, while at low frequencies, the Warburg impedance is generated. Thus, the EIS spectra include a semicircle at high frequencies, corresponding to the electron transfer limiting process, and a linear part (with large angle with respect to real impedance axis or almost parallel to imaginary impedance axis) at low frequencies resulting from the diffusion limiting step of the electrochemical process. According to theory, the straight line interprets a faster mass transfer-limited process due to electron flow from electrode surface to the bulk solution (occurring at lower frequencies), whereas, the semicircular portion describes a relatively slower charge transfer-limited process (taking place at higher frequencies). Among P-MWCNTs composite films studied, P-MWCNTs-2, P-MWCNTs-3, and P-MWCNTs-4 exhibit in their Nyquist plots an obvious semicircle (its diameter differs for each P-MWCNTs film) in the high-frequency region of the impedance spectra and a straight line in the low-frequency region. However, the Nyquist plot of P-MWCNTs-1 exhibits a depressed very small semicircle (with small diameter) that is almost invisible and a linear (straight) ion diffusion portion having the greatest slope compared to the other novel P-MWCNTs composite films studied (the slope of the liner portion is actually very close to the slope of the imaginary impedance axis). These findings imply that among the films studied, P-MWCNTs-1 exhibits the greatest conductivity or the lowest internal resistance including polarization impedance. According to literature, the absence of semicircle in the complex impedance plane was explained by means of high ionic conductivity at the electrode/electrolyte interface [35]. These findings indicate that the electrochemical quality of P-MWCNTs-1 appears to be better. The extracted impedance data were satisfactorily fitted to the Randles equivalent electrical circuit $(R_s+(C_{dl}/(R_{ct}+Z_w)))$ (software Thales, version 4.15). The Randles circuit is used frequently as equivalent electrical model to interpret experimental EIS spectra and includes an uncompensated solution resistance (R_s) connected in series to a parallel combination of double-layer capacitance (C_{dl}) and charge transfer resistance at the electrode/solution interface (R_{ct}) in series with Warburg diffusion impedance (Z_w) [36]. The electrical circuit used for simulation was found to fit satisfactorily the impedance data. The mean and maximum modified impedance errors resulted from the simulation process were estimated in all cases to be less than 0.3 % and 2.5 %, respectively, which can be considered quite acceptable. It must be mentioned that to obtain acceptable reproduction of experimental impedance data, the capacitor was

replaced by constant phase element. The explanation for the presence of constant phase element is the microscopic roughness of the surface of carbon nanotube-based films that causes an inhomogeneous distribution in solution resistance and double-layer capacitance. As it can be seen in Fig. 5, the intercept between the impedance spectrum and the real impedance axis was very small (between 3 and 6 Ω) for all investigated composite films. The small intercept demonstrates that the series resistance (R_s), which includes the electrolyte solution resistance and the contact resistance at the interface of active material/current collector, was quite small for all different P-MWCNTs composite films studied.

The most suitable impedance parameter for further evaluation of the electrochemical features and for studying the interfacial properties of P-MWCNTs composite films is the charge transfer resistance (R_{ct}). This impedance parameter controls the electron transfer kinetics of redox system at electrode interface and represents the barrier for the electron transfer process occurring onto electrode's surface [37]. In other words, R_{ct} represents the hindering behavior of interface properties of the electrode and it can be estimated from the diameter of capacitive semicircle in Nyquist plots (in high frequencies) by extrapolating the semicircle to the real impedance axis [38].

The absence of semicircle in Nyquist plot of P-MWCNTs-1 demonstrates that the charge transfer resistance of this particular film is the smallest among the P-MWCNTs composite films studied. For this particular film, the phase angle increases continuously with the decrease of frequency (the straight line is almost parallel to imaginary impedance axis) indicating that the kinetic and charge transfer are no longer rate-determining steps, while the mass transfer (capacitance) remains the dominant component of impedance of the system. In contrast to P-MWCNTs-1, on other composite films such as P-MWCNTs-2, P-MWCNTs-3, and P-MWCNTs-4, semicircles can be obviously seen with different diameters indicating that onto these films, the charge transfer process is the rate determining step.

The R_{ct} values estimated for $[Fe(CN)_6]^{3-/4-}$ on various P-MWCNTs films resulted from the simulation of experimental impedance data are included in Table 2 for comparison reasons. The findings demonstrate that the R_{ct} values, and thus the barrier for electron transfer, tend to decrease with the following order: P-MWCNTs-3>P-MWCNTs-2>P-MWCNTs-4>P-MWCNTs-1. The impedance results are in absolute agreement with those extracted from CV studies. Namely, the kinetic parameter k_s estimated for $[Fe(CN)_6]^{3-/4-}$ on various P-MWCNTs composite films tends to increase with the same order: P-MWCNTs-3 < P-MWCNTs-2 < P-MWCNTs-4 < P-MWCNTs-1, confirming that the charge transfer

resistance is inversely proportional to the exchange current and, thus, to the heterogeneous electron-transfer rate constant of redox system [39]. As was already reported above, with the same order, the detection ability of the P-MWCNTs composite films towards $[Fe(CN)_6]^{3-/4-}$ tends to increase. The charge transfer resistance, the rate of electron transfer, the lower limit of detection, and the sensitivity of various P-MWCNTs composite films towards $[Fe(CN)_6]^{3-/4-}$ are presented graphically in histograms shown in Fig. 6. From the histograms, it can be clearly seen that within the films fabricated, the P-MWCNTs-1

film possesses the smallest charge transfer resistance, the greatest rate for electron transfer, the lowest limit of detection, and, consequently, the highest sensitivity towards $[Fe(CN)_6]^{3-/4-}$. In addition, within the P-MWCNTs films tested, P-MWCNTs-3 reveals the slowest charge transfer kinetic, the greatest barrier for electron transfer, and, consequently, the lowest detection ability. By considering the results extracted from SEM and TEM analysis, it can be concluded that the P-MWCNTs films consisting of long and sole carbon nanotubes exhibit faster response and greater sensitivity compared to those

Fig. 6 Histograms showing the charge-transfer resistance (a), electron-transfer rate constant (b), lower limit of detection (c), and sensitivity (d) of P-MWCNTs-1 (I), P-MWCNTs-2 (II), P-MWCNTs-3 (III), and P-MWCNTs-4 (IV) composite films towards $Fe(CN)_6]^{3-/4-}$ (1.0 M KCl)
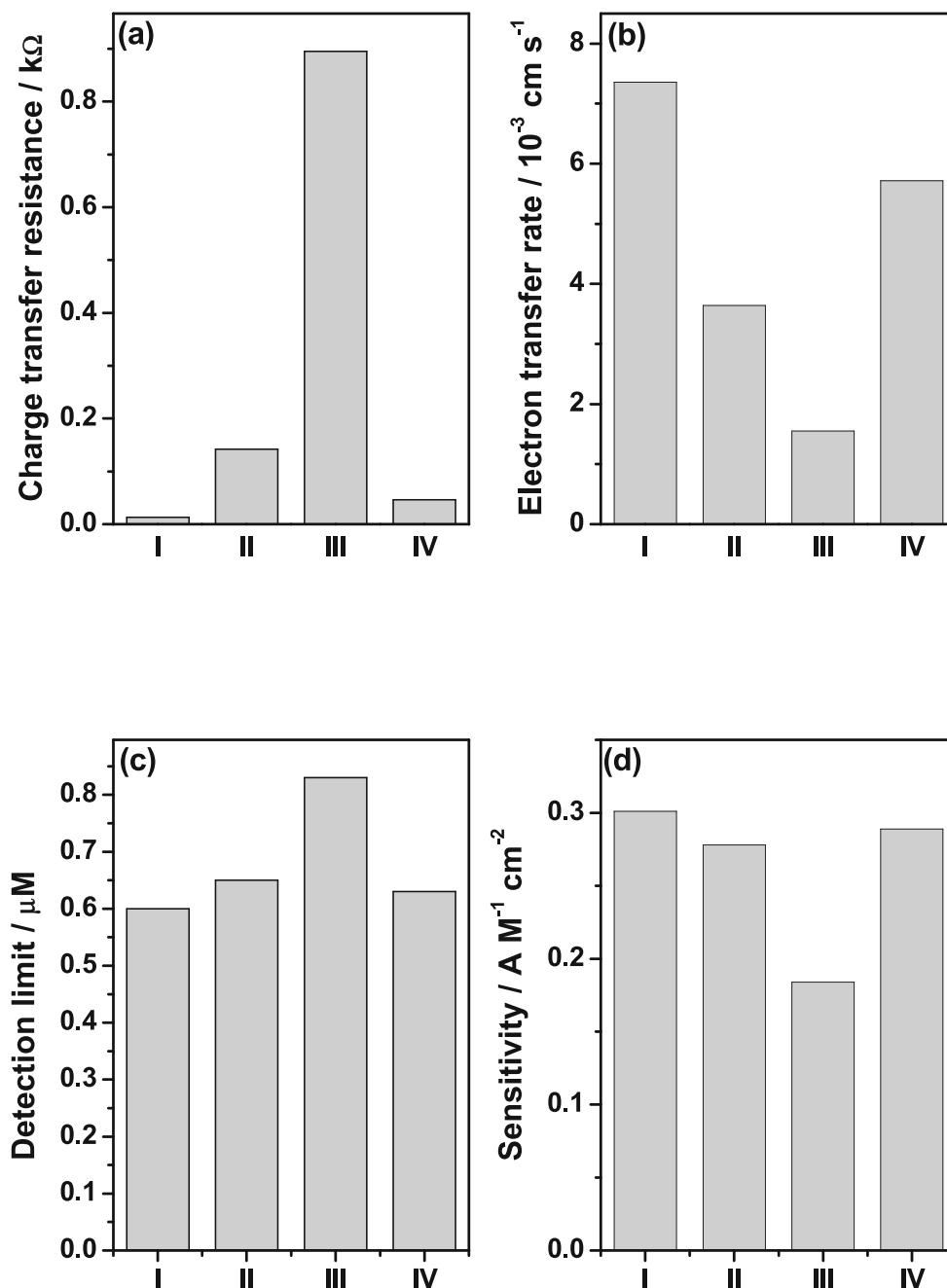
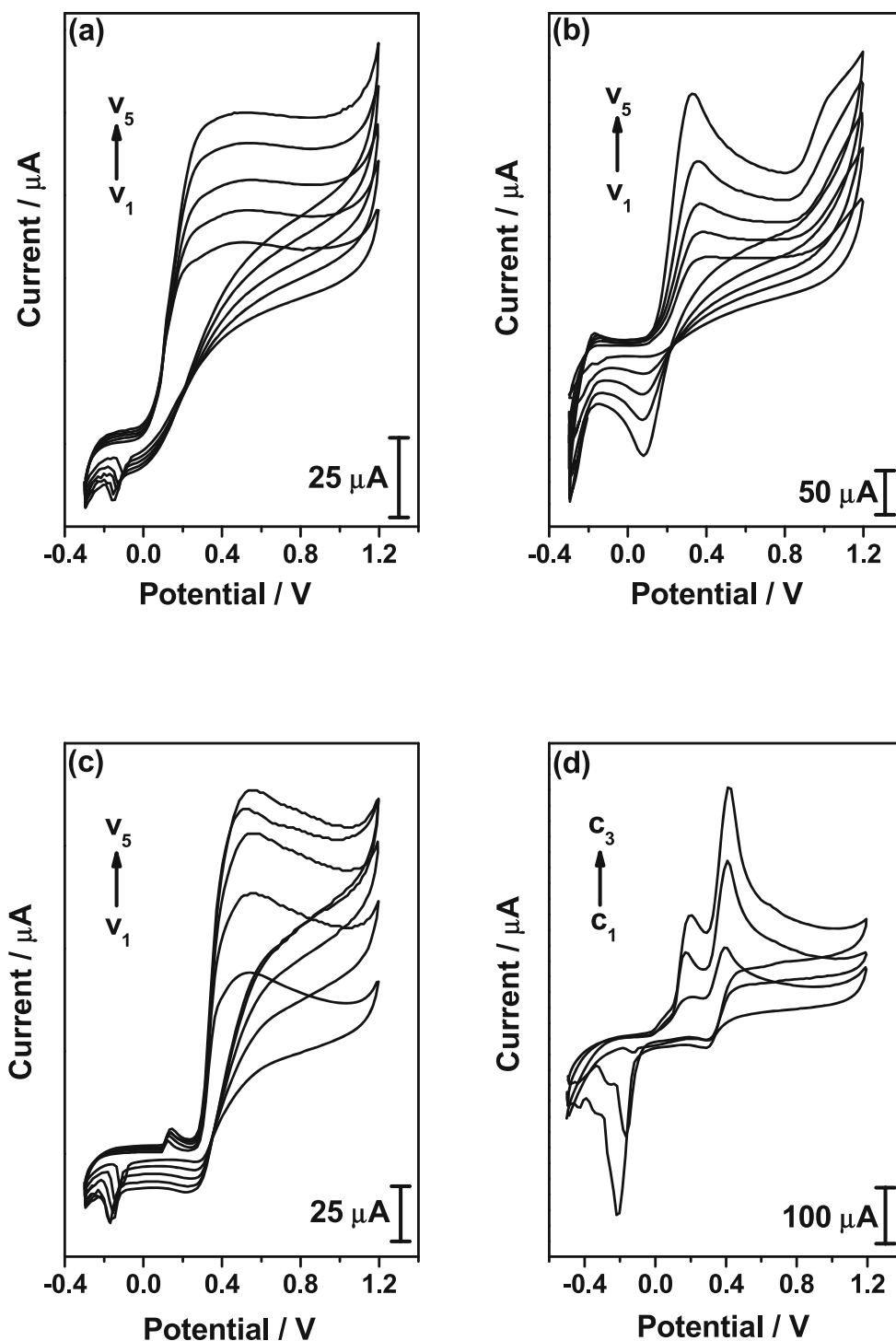**Fig. 7** CVs recorded for AA (**a**), DA (**b**), UA (**c**), and AA/UA binary mixtures (**d**) on P-MWCNTs-1 composite film (PBS, pH 7.0). The CVs shown in **a**, **b**, and **c** (from inner to outer) were recorded at the scan rates of $v_1=0.02$ V·s^{-1}, $v_2=0.04$ V·s^{-1}, $v_3=0.06$ V·s^{-1}, $v_4=0.08$ V·s^{-1}, and $v_5=0.10$ V·s^{-1}, while the CVs shown in **d** (from inner to outer) were recorded with AA:UA concentration ratios of 1:1 (c_1), 1:2 (c_2), and 1:3 (c_3) at the scan rate of $v_1=0.02$ V·s^{-1}

containing clustered carbon nanotubes. The results obtained are quite promising and clearly demonstrate that the novel P-MWCNTs are suitable to be used as electrodes in electrochemical sensing.

The response of P-MWCNTs-1 film towards oxidation of molecules with biological interest, such as AA, UA, and DA, was tested in phosphate buffer solutions (PBS) at pH 7.0 in the concentration range of 0.030–0.238 mM

and the scan rate range of 20–100 mV s^{-1}. Representative CVs recorded at various scan rates for AA, DA, and UA are shown in Figs. 7a–c. The electrochemistry measurements were performed at pH 7.0 since it is very close to the physiological pH (pH 7.365). Furthermore, it was verified that at pH 7.0, the voltammetric response of the P-MWCNTs-1 film towards oxidation of AA, UA, and DA appears to be enhanced. From the recorded CVs, it can be

Table 3 Lower limit of detections (LOD) of pristine MWCNTs, P-MWCNTs, and N-MWCNTs composite films towards oxidation of AA, DA, and UA (PBS, pH 7.0)

Analyte	LOD/μM		
	MWCNTs	P-MWCNTs	N-MWCNTs
AA	1.40[a]/8.0[b]	1.12	0.97[c]
DA	0.30[d]/0.2[b]	0.19	0.03[d]
UA	1.0[b]	0.80	0.54[c]

[a] Ref. [42]

[b] Ref. [43]

[c] Ref. [40]

[d] Ref. [13]

seen that the oxidation of AA, DA, and UA onto P-MWCNTs-1 occurs at about +0.348 V, +0.409 V, and +0.554 V (vs. Ag/AgCl), respectively. The findings demonstrate that the oxidation overpotential of AA onto P-MWCNTs appears to be about ~226 mV more anodic (more positive) compared to that measured onto N-MWCNTs (+0.122 V vs. Ag/AgCl) and about 38 mV less anodic (less positive) compared to that measured onto pristine MWCNTs (+0.386 V vs. Ag/AgCl) [40]. It is interesting to mention that the overpotential of AA measured onto P-MWCNTs is significantly less anodic compared to that measured on conventional platinum electrode. The results clearly indicate that there is slight diminishing of overpotential of AA onto P-MWCNTs compared to that measured onto pristine MWCNTs. However, P-MWCNTs cannot compete the great diminishing of overpotential of AA that occurs onto N-MWCNTs. This finding confirms once more the improved ability of carbon nanotubes that incorporate nitrogen into their structure to lower the overpotential of redox systems [41]. Consequently, since the oxidation potential of DA lies very close to that of AA (the oxidation potential of DA is about 61 mV more positive compared to that of AA), there is strong interference of DA in voltammetric detection of AA and, likewise, there is an interference of AA in the detection of DA. However, since the potential difference between the oxidation waves of AA and UA is relative large (greater than 200 mV), their simultaneous voltammetric analysis can be carried out onto P-MWCNTs-1 composite film, but only in the absence of DA. Thus, in CVs recorded for AA/UA binary system with concentration ratios 1:1, 1:2, and 1:3, the oxidation waves of AA and UA are well separated (~210 mV) permitting therefore their simultaneous analysis (Fig. 7d). The lower limits of detection estimated for P-MWCNTs towards oxidation of AA, DA, and UA are reported for comparison reasons along with those obtained on pristine and nitrogen-doped MWCNTs in Table 3. An extensive comparison of limits of detection obtained in the present work for P-

MWCNTs towards AA, DA, and UA with those reported in literature for other novel composite films is shown in Figure S3 (Supporting Information). As it can be seen, the detection ability of the films towards oxidation of studied biomolecules tends to enhance with the following order: MWCNTs<P-MWCNTs<N-MWCNTs demonstrating that the phosphorus doping improves the sensitivity of the carbon nanotubes; however, the electrocatalytic properties of nitrogen-doped nanotubes appear to be slightly more improved. Furthermore, P-MWCNTs appears to be significantly more sensitive compared to other novel composite films reported in literature demonstrating that P-MWCNTs is quite a promising material for further applications in electrochemical biosensing.

Conclusions

In the present work, P-MWCNTs were fabricated on silicon/silicon oxide substrate with decomposition of CyH and TPP in the presence of $FeCp_2$. For the fabrication process, the mass percent of TPP in TPP/CyH/$FeCp_2$ ternary mixture was varied from 0.5 % to 2.0 % wt., while that of $FeCp_2$ was fixed to either 2 % or 5 % wt. The novel P-MWCNTs films were characterized by means of SEM and TEM in combination with EDX and by Raman spectroscopy. In addition, the P-MWCNTs composite films were electrochemically investigated with respect to their response to $[Fe(CN)_6]^{3-/4-}$ (KCl, 1.0 M). The electron microscopy analysis demonstrate that the P-MWCNT films include nanotubes that possess two different types of configuration, namely, they consist of either sole and long carbon nanotubes or nanotubes adducts (clusters) along with nanotube "onions". The structure of P-MWCNTs is somehow analogous to the bamboo-shaped structure of nitrogen-doped MWCNTs. Electrochemical studies reveal that the films consisting of non-clustered sole carbon nanotubes exhibit slightly faster response and enhanced sensitivity towards $[Fe(CN)_6]^{3-/4-}$ compared to those contain adducts (clusters) of carbon nanotubes. The P-MWCNTs films were found to be suitable for the analysis of AA, DA, and UA with limits of detection of 1.12, 0.19, and 0.80 μM, respectively. The findings exhibit that P-MWCNTs is a quite capable material for applications in electrochemical sensing.

References

1. Bernholc J, Brenner D, Buongiorno Nardelli M, Meunier V, Roland C (2002) Mechanical and electrical properties of nanotubes. Annu Rev Mater Res 32:347–375

2. Luo H, Shi Z, Li N, Gu Z, Zhang Q (2001) Investigation of the electrochemical and electrocatalytic behavior of single-wall carbon nanotube film on a glassy carbon electrode. Anal Chem 73:915–920

3. Musamech M, Wang J, Merkoci A, Lin YH (2002) Low-potential stable NADH detection at carbon-nanotube-modified glassy carbon electrodes. Electrochem Commun 4:743–746

4. Yu J, Zhao J, Hu C, Hu S (2007) Enhanced oxidation of estrone at multi-wall carbon nanotubes film electrode: direct evidence for the advantage of carbon nanotubes over other carbonaceous materials. J Nanosci Nanotechnol 7:1631–1638

5. Xie X, Gan T, Sun D, Wu K (2008) Application of multi-walled carbon nanotubes/nafion composite film in electrochemical determination of Pb^{2+}. Fuller Nanotub Carbon Nanostruct 16:103–113

6. Brahman PK, Dar RA, Tiwari S, Pitre KS (2012) Electrochemical behavior of gatifloxacin at multi-walled carbon nanotube paste electrode and its interaction with DNA. Rev Anal Chem 31:83–92

7. Debnarayan J, Chia-Liang S, Li-Chyong C, Kuei-Hsien C (2013) Effect of chemical doping of boron and nitrogen on the electronic, optical, and electrochemical properties of carbon nanotubes. Prog Mater Sci 58:565–635

8. Liu H, Zhang Y, Li R, Sun X, Abou-Rachid H (2012) Thermal and chemical durability of nitrogen-doped carbon nanotubes. J Nanoparticle Res 14:1016 (8 Pages)

9. Maciel IO, Campos-Delgado J, Cruz-Silva E, Pimenta MA, Sumpter BG, Meunier V, Lopez-Urias F, Munoz-Sandoval E, Terrones H, Terrones M, Jorio A (2009) Synthesis, electronic structure, and Raman scattering of phosphorus-doped single-wall carbon nanotubes. Nano Lett 9:2267–2272

10. Cruz-Silva E, Cullen DA, Gu L, Romo-Herrera JM, Munoz-Sandoval E, Lopez-Urias F, Sumpter BG, Meunier V, Charlier JC, Smith DJ, Terrones H, Terrones M (2008) Heterodoped nanotubes: theory, synthesis, and characterization of phosphorus-nitrogen doped multiwalled carbon nanotubes. ACS Nano 2:441–448

11. Cruz-Silva E, Lopez-Urias F, Munoz-Sandoval E, Sumpter BG, Terrones H, Charlier JC, Meunier V, Terrones M (2009) Electronic transport and mechanical properties of phosphorus- and phosphorus-nitrogen-doped carbon nanotubes. ACS Nano 3:1913–1921

12. Tsierkezos NG, Ritter R (2010) Synthesis and electrochemistry of multiwalled carbon nanotube films directly attached on silica substrate. J Solid State Electrochem 14:1101–1107

13. Tsierkezos NG, Ritter R (2012) Oxidation of dopamine on multiwalled carbon nanotubes. J Solid State Electrochem 16:2217–2226

14. Tsierkezos NG, Wetzold N, Ritter U (2013) Electrochemical responses of carbon nanotubes-based films printed on polymer substances. Ionics 19:335–341

15. Tsierkezos NG, Wetzold N, Ritter U, Hübler AC (2013) Analysis of dopamine on printed polymer thin film consisting of multi-walled carbon nanotubes. Monatsh Chem 144:581–588

16. Tsierkezos NG, Wetzold N, Ritter U, Hübler AC (2013) Preparation and electrochemical performance of novel printed film consisting of multi-walled carbon nanotubes. J Nanosci Lett 3:6 (6 pages)

17. Tsierkezos NG, Wetzold N, Hübler AC, Ritter U, Szroeder P (2013) Multi-walled carbon nanotubes printed onto polycarbonate substrate for electrochemical sensing. Sens Lett 11:1465–1471

18. Tsierkezos NG, Ritter U (2011) Application of electrochemical impedance spectroscopy for characterisation of the reduction of benzophenone in acetonitrile solutions. Phys Chem Liq 49:729–742

19. Jourdain V, Stéphan O, Castignolles M, Loiseau A, Bernier P (2004) Controlling the morphology of multiwalled carbon nanotubes by sequential catalytic growth induced by phosphorus. Adv Mater 16:447–453

20. Larrude DG, Maia da Costa MEH, Monteiro FH, Pinto AL, Freire FL Jr (2012) Characterization of phosphorus-doped multiwalled carbon nanotubes. J Appl Phys 111:064315 (6 pages)

21. Wang H, Wang H, Chen Y, Liu Y, Zhao J, Cai Q, Wang X (2013) Phosphorus-doped graphene and (8, 0) carbon nanotube: structural, electronic, magnetic properties, and chemical reactivity. Appl Surf Sci 273:302–309

22. Ritter U, Scharff P, Siegmund C, Dmytrenko OP, Kulish NP, Prylutskyy YI, Belyi NM, Gubanov VA, Komarova LI, Lizunova SV, Poroshin VG, Shlapatskaya VV, Bernas H (2006) Radiation damage to multi-walled carbon nanotubes and their Raman vibrational modes. Carbon 44:2694–2700

23. Ritter U, Scharff P, Dmytrenko OP, Kulish NP, Prylutskyy YI, Belyi NM, Gubanov VA, Komarova LA, Lizunova SV, Shlapatskaya VV, Bernas H (2007) Radiation damage and Raman vibrational modes of single-walled carbon nanotubes. Chem Phys Lett 447:252–256

24. Tuinstra F, Koenig J (1970) Raman spectrum of graphite. J Chem Phys 53:1126–1130

25. Ferrari A, Robertson J (2000) Interpretation of Raman spectra of disordered and amorphous carbon. Phys Rev B 61:14095–14107

26. Szroeder P, Górska A, Tsierkezos N, Ritter U, Strupiński W (2013) The role of band structure in electron transfer kinetics in low-dimensional carbon. Materialwiss Werkst 44:226–230

27. Benissad-Aissani F, Aı̈t-Amar H, Schouler MC, Gadelle P (2004) The role of phosphorus in the growth of vapour-grown carbon fibres obtained by catalytic decomposition of hydrocarbons. Carbon 42:2163–2168

28. Wen YH, Zhang HM, Qian P, Zhou HT, Zhao P, Yi BL, Yang YS (2006) A study of the Fe(III)/Fe(II)-triethanolamine complex redox couple for redox flow battery application. Electrochim Acta 51:3769–3776

29. Solak AO, Eichorst LR, Clark WJ, McCreery RL (2003) Modified carbon surfaces as 'organic electrodes' that exhibit conductance switching. Anal Chem 75:296–305

30. Nicholson RS, Shain I (1964) Theory of stationary electrode polarography: single scan and cyclic methods applied to reversible, irreversible, and kinetic systems. Anal Chem 36:706–723

31. Tsierkezos NG, Ritter U (2012) Influence of concentration of supporting electrolyte on electrochemistry of redox systems on multi-walled carbon nanotubes. Phys Chem Liq 50:661–668

32. Gong K, Du F, Xia Z, Durstock M, Dai L (2009) Nitrogen-doped carbon nanotube arrays with high electrocatalytic activity for oxygen reduction. Science 323:760–764

33. Tang Y, Allen BL, Kauffman DR, Star A (2009) Electrocatalytic activity of nitrogen-doped carbon nanotube cups. J Am Chem Soc 131:13200–13201

34. Min YS, Bae EJ, Kim UJ, Lee EH, Park N, Hwang CS, Park W (2008) Unusual transport characteristics of nitrogen-doped single-walled carbon nanotubes. Appl Phys Lett 93:043113 (3 pages)

35. Li X, Rong J, Wei B (2010) Electrochemical behavior of single-walled carbon nanotube supercapacitors under compressive stress. ACS Nano 4:6039–6049

36. Prodromidis MI (2010) Impedimetric immunosensors—a review. Electrochim Acta 55:4227–4233

37. Barsoukov E, Macdonald JR (2005) Impedance spectroscopy: theory, experiment, and applications: John (Wiley and Sons)

38. Peng H, Ma G, Mu J, Sun K, Lei Z (2014) Low-cost and high energy density asymmetric supercapacitors based on polyaniline nanotubes and MoO$_3$ nanobelts. J Mater Chem A 2:10384–10388

39. Chirea M (2013) Electron transfer at gold nanostar assemblies: a study of shape stability and surface density influence. Catalysts 3: 288–309

40. Tsierkezos NG, Ritter U (2012) Simultaneous detection of ascorbic acid and uric acid at MWCNT modified electrodes. J Nanosci Lett 2: 25 (14 pages)

41. Goran JM, Favela CA, Stevenson KJ (2013) Electrochemical oxidation of dihydronicotinamide adenine dinucleotide at nitrogen-doped carbon nanotube electrodes. Anal Chem 85: 9135–9141

42. Kumar S, Vicente-Beckett V (2012) Glassy carbon electrodes modified with multiwalled carbon nanotubes for the determination of ascorbic acid by square-wave voltammetry. Beilstein J Nanotechnol 3:388–396

43. Kamyabi MA, Narimani O, Monfared HH (2011) Electroless deposition of bis(4'-(4-pyridyl)-2,2':6',2"-terpyridine)iron(II) thiocyanate complex onto carbon nanotubes modified glassy carbon electrode: application to simultaneous determination of ascorbic acid, dopamine and uric acid. J Braz Chem Soc 22:468–477